# SCIENTIFIC REP☼RTS

# Hydrogen Impurity Defects in Rutile TiO₂

Li-Bin Mo[1], Yu Wang[2], Yang Bai[1], Qing-Yun Xiang[1], Qun Li[1], Wen-Qing Yao[3], Jia-Ou Wang[4], Kurash Ibrahim[4], Huan-Hua Wang[4], Cai-Hua Wan[5] & Jiang-Li Cao[1]

Hydrogen-related defects play crucial roles in determining physical properties of their host oxides. In this work, we report our systematic experimental and theoretical (based on density functional theory) studies of the defect states formed in hydrogenated-rutile TiO₂ in gaseous H₂ and atomic H. In gas-hydrogenated TiO₂, the incorporated hydrogen tends to occupy the oxygen vacancy site and negatively charged. The incorporated hydrogen takes the interstitial position in atom-hydrogenated TiO₂, forming a weak O-H bond with the closest oxygen ion, and becomes positive. Both states of hydrogen affect the electronic structure of TiO₂ mainly through changes of Ti 3d and O 2p states instead of the direct contributions of hydrogen. The resulted electronic structures of the hydrogenated TiO₂ are manifested in modifications of the electrical and optical properties that will be useful for the design of new materials capable for green energy economy.

Hydrogen has rather complex chemical states in nature including $H^+$, $H^0$ and $H^-$, which makes its behaviors in the host materials complicated. A fuller understanding of the interactions between oxide materials and hydrogen is crucial for the research and successful applications of such materials in a broad range of scientific and technological fields from green energy techniques to electronics industries. For example, hydrogen ions are positively charged in ZnO, contributing to high conductivity[1,2]. In BaTiO₃, instead, hydrogen ions are negatively charged, occupying the position of oxygen vacancies[3]. As-doped BaTiO₃₋ₓHₓ is also electronically conductive and stable in air and water at ambient conditions[3]. It is also proposed that new materials or devices with novel functionalities may be designed through appropriate hydrogen treatment. All these areas are calling for a thorough understanding of the hydrogen behaviors in oxide materials and responses of the hosts to different hydrogen atmospheres.

TiO₂ shows promising application prospects in some rapidly growing hydrogen-related technologies such as hydrogen production[4,5], and solar cells[6], etc[7–9] because of its excellent properties and ready accessibility. For example, Chen et al.[10] reported that hydrogenated anatase TiO₂ nanocrystals exhibited significantly improved solar photocatalytic performances, which triggered much research interest in the hydrogen defect engineering of oxide materials. Furthermore, hydrogenated TiO₂ nanowire arrays also possess excellent photoelectrochemical-water-splitting performance[11] and super capacitive properties[12]. Interestingly, besides of high-temperature annealing in gaseous H₂, treatment by atomic H at room temperatures could also significantly change performances of TiO₂. Chester[13] first found that the conductivity of TiO₂ increased upon atom-hydrogenation through water electrolysis. Chen[14] also observed similar effects in TiO₂ and other oxides. But the proposed mechanisms for the above behaviors diverge in different researches. Chen[10,15] and Naldoni[16] regarded surface disorders induced narrowing of bandgap of TiO₂ and therefore the enhancement of its absorption ratio in visible light range. Deford[17], Herklotz[18] and Kilici[19] assumed that the interstitial hydrogen was formed in gas-hydrogenated TiO₂ and correlated the interstitial hydrogen with the increase in conductivity and light absorption. Besides of the viewpoint

[1]Institute of Advanced Materials and Technology, Beijing Key Lab for Corrosion, Erosion and Surface Technology, University of Science and Technology Beijing, Beijing 100083, China. [2]Department of Applied Physics, Hong Kong Polytechnic University, Hong Kong, China. [3]Department of Chemistry, Tsinghua University, Beijing 100084, China. [4]Institute of High Energy Physics, Chinese Academy of Sciences, Beijing 100049, China. [5]Institute of Physics, Chinese Academy of Sciences, Beijing 100190, China. Correspondence and requests for materials should be addressed to J.-L.C. (email: perov@sina.com)
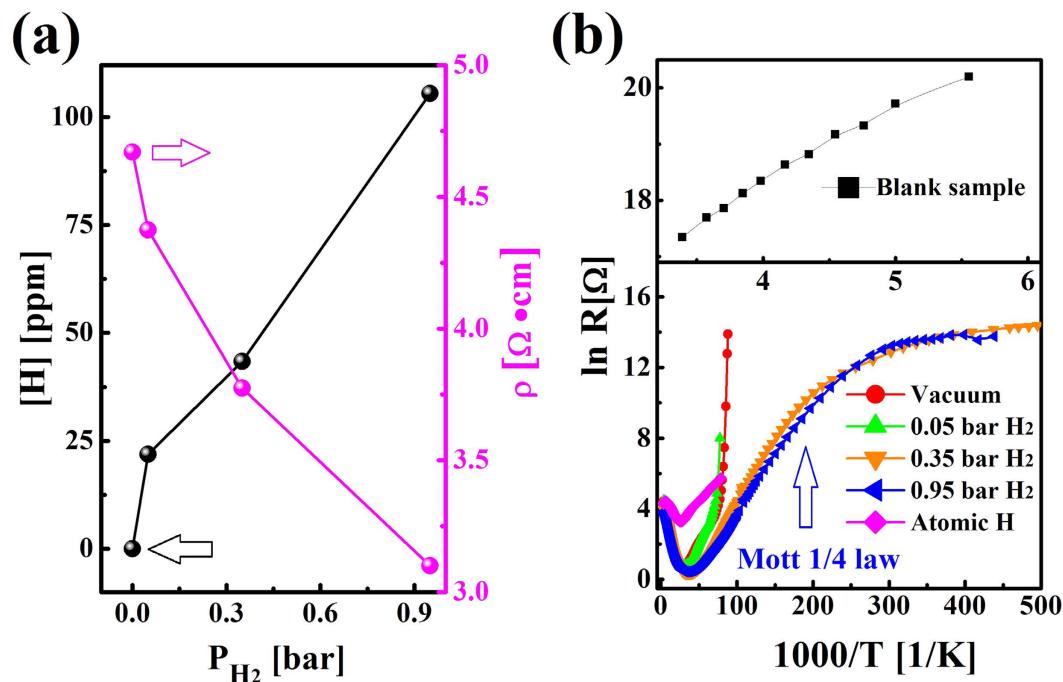
**Figure 1. Molar content of incorporated hydrogen and transport properties of hydrogenated $TiO_2$ single crystals. (a)** Changes of the hydrogen content and RT resistivity of $TiO_2$ with $P_{H2}$ upon gas-hydrogenation. An oxygen loss of about 300 ppm is measured for the 0.95 bar gas-hydrogenated rutile $TiO_2$, which is approximately 3 times of the hydrogen content. **(b)** temperature-dependences of resistivity from 2 K to 300 K.

that interstitial hydrogen atom was the origin of enhanced conductivity in atom-hydrogenated $TiO_2$, Chester[13] and Chen[14] also regarded that $V_O$ formed in oxide materials in hydrogen atmospheres[20–23]. Wang[11] and Zhai[24], however, regarded that $V_O$ was the main reason responsible for the reduction of bandgap. Even more complex, Lu et al.[12] thought that the surface hydroxyl groups of hydrogenated $TiO_2$ should be responsible for the change of performances. Filippone et al.[25] reported that H behaved as a deep donor in rutile and formed stable H-oxygen vacancies ($V_O$) complexes. Though the defect engineering by hydrogen treatment has attracted much attention over recent years, the defect states and their atomic- and electronic structure in hydrogenated $TiO_2$ are still not clearly understood so far. The above debate is partially induced, we think, by different sample structures (nano-particles, nanowires or bulk materials) and/or by different treatment conditions (high temperature annealing or room temperature electrochemical method) among different research groups. In this research, we focus only on bulk materials with single crystalline to first minimize the influence of surface disorder. Further, we applied the above two methods to treat the same batch of samples to minimize influence of diversity among different samples. The above controlled conditions will make our data more comparative and suggestive to dissolve some basic questions in this field Therefore, the present study aims at exploring the hydrogen impurity-related defect states in bulk rutile $TiO_2$. Oxygen vacancies and H-oxygen vacancies ($V_O$) complexes as main defects in gas-hydrogenated $TiO_2$ were introduced through high-temperature annealing treatment and interstitial hydrogen as main defects in atom-hydrogenated $TiO_2$ were introduced by water electrolysis. Through comparison experiments with bulk $TiO_2$ samples with different defects as well as density functional theory (DFT) calculations, we hope to open up new opportunities in green energy techniques, including water splitting, dye-sensitized solar cells, and photocatalysis etc.

Figure 1 (a) shows hydrogen contents and room temperature (RT) resistivity of gas-hydrogenated rutile $TiO_2$. The samples treated with $P_{H2} = 0$ were named as vacuum-annealed samples. Their resistivity decreases by more than seven orders of magnitude to several $\Omega$ cm, which could be attributed to the formation of $V_O$[22,23]. With increasing $P_{H2}$ the incorporated hydrogen content increases and resistivity decreases monotonically. Hall measurements show that the carriers in these high temperature-annealed samples are all electrons (Supplemental Fig. S1), demonstrating formation of donor defects. Carrier mobility in the 0.95 bar gas-hydrogenated sample is 42.3 cm$^2$ V$^{-1}$ s$^{-1}$ at 30 K, lower than 94.5 cm$^2$ V$^{-1}$ s$^{-1}$ of the vacuum-annealed sample. Fig. 1(b) plots the temperature-dependence of the resistivity between 2 K and 300 K. Different from the blank sample, the resistivity of the high temperature-annealed samples first decreases with decreasing temperature and then increases sharply after reaching a minimum around 30 K. Here, the temperature dependence of the resistivity above 30 K is proposed to be determined mainly by the carrier mobility. Below 30 K, the donors start to be frozen out from conduction band (CB). The resistivity exhibits an exponential dependence on 1/T, following the equation $\rho = \rho_0 \exp(-\Delta E_D / k_B T)$[26].
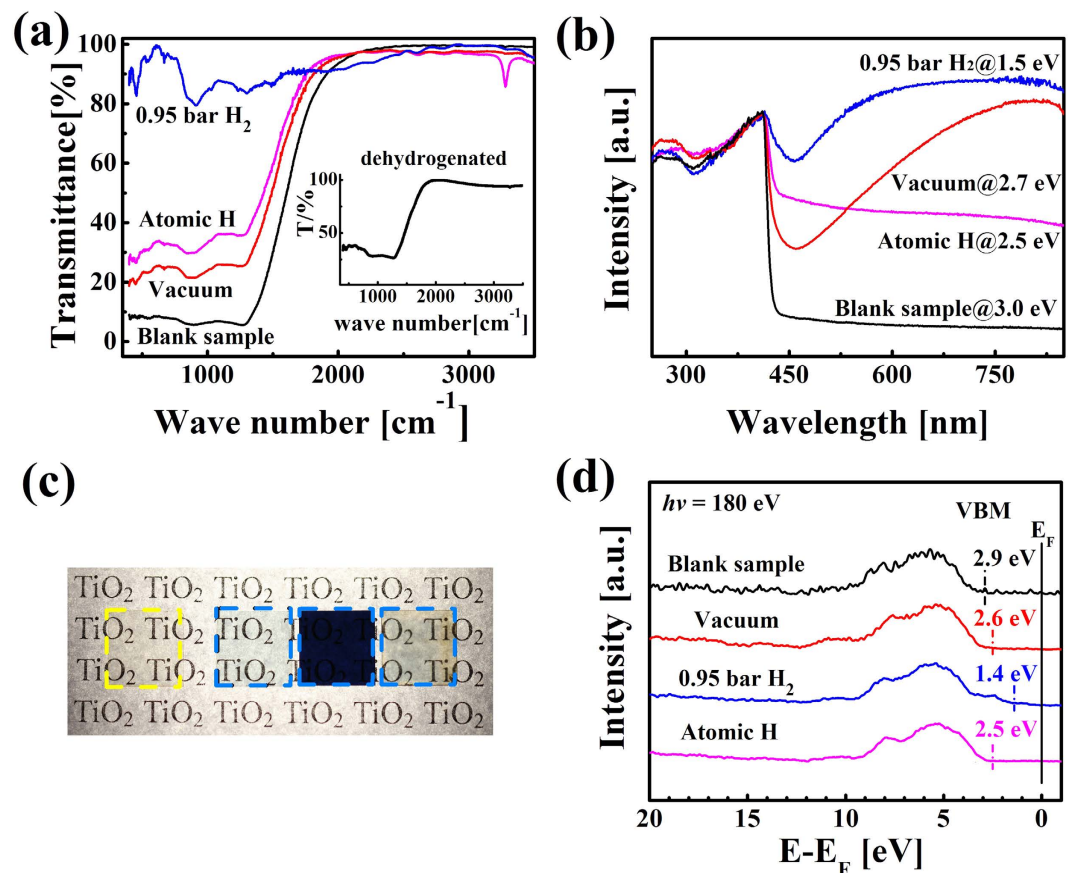
**Figure 2. Characterizations of TiO$_2$ single crystals. (a)** FTIR absorption spectra. The inset shows the FTIR spectrum of the atom-hydrogenated TiO$_2$ after a 10 min-dehydrogenation at 700 °C. **(b)** Optical absorption spectra. The band gap values are given. **(c)** Optical images of the blank, vacuum-annealed, gas-hydrogenated and atom-hydrogenated samples (from left to right). **(d)** Valence-band spectra of synchrotron radiation.

And fittings show that the ionization energy of defects $\Delta E_D$ of all high temperature-annealed samples are $6.5 \pm 1.5$ meV. It indicates that their dominant defects could be the same, i.e. $V_O$. Similarly, Yagi[23] *et al.* reported a $\Delta E_D$ of ~5 meV for $V_O$ in rutile TiO$_2$. The resistivity of the samples annealed in 0.35 and 0.95 bar H$_2$ at high temperature increases with further decreasing temperature, following Mott's law $\rho = \rho_1 \exp(T_0/T)^{1/4}$. Their conductivity mechanism could be attributed to the variable range hopping conduction[26,27]. The higher $P_{H2}$ leads to a higher donor density and finally produces a defect band in the band gap. Consequently, electrons could hop between donors through thermal-assisted tunneling, which answers for the residual conductivity below 4 K in the higher $P_{H2}$-hydrogenated TiO$_2$.

TiO$_2$ single crystals with interstitial H (H$_i$) defects fabricated by atom hydrogenation at RT show a much reduced RT resistivity of $14.5\,\Omega$ cm and a similar temperature-dependence with the high temperature-annealed samples (Fig. 1b). The $\Delta E_D$ of atom-hydrogenated TiO$_2$ has not been reported before. Here, a shallow donor level with a $\Delta E_D$ of 3.9 meV is measured, smaller than that in the high temperature-annealed samples. Thus, it is inferred that the defects in atom-hydrogenated TiO$_2$ are different from those in gas-hydrogenated TiO$_2$. Furthermore, carrier mobility of the atom-hydrogenated sample is 7.71 cm$^2$ V$^{-1}$ s$^{-1}$ (Supplemental Fig. S1), much smaller than that of vacuum-annealed sample and that of gas-hydrogenated TiO$_2$, which further indicates different scattering defects in samples treated by the different methods.

Figure 2a shows the Fourier transform infrared (FTIR) absorption spectra. The blank sample has strong absorption between $400 \sim 1300$ cm$^{-1}$ as normal[28,29]. In contrast, the transparency of hydrogenated samples increases significantly. Interestingly, the 0.95 bar gas-hydrogenated sample becomes almost completely infrared transparent in the full range of measurement. Note that the gas-hydrogenated TiO$_2$ also has high conductivity and could be potentially used as transparent conductors in the infrared band. A strong absorption peak at 3280 cm$^{-1}$ is observable for the atom-hydrogenated sample. This peak should be the stretch mode of O-H bonds in rutile TiO$_2$[18,28]. The O-H absorption peak in atom-hydrogenated TiO$_2$ disappears after a 10 min-dehydrogenation in air at 700 °C, as shown in the inset of Fig. 2a. Furthermore, high resistivity of the atom-hydrogenated TiO$_2$ recovered gradually to the virgin state after a few days aging at RT, similar with previous report[30], whereas little changes can be observed in the gas-hydrogenated
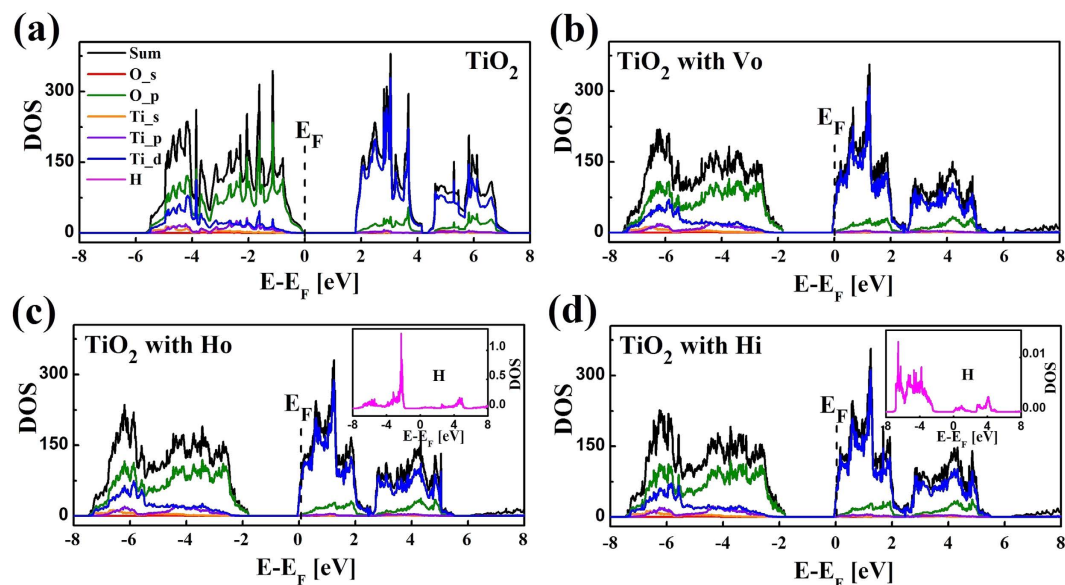
**Figure 3. DFT calculations.** The DOS and PDOS of (**a**) the perfect rutile $TiO_2$ and (**b**) $TiO_2$ with $V_O$ in simulation of vacuum-annealed $TiO_2$. In our calculations, the intrinsic band gap of rutile $TiO_2$ is 1.7 eV, in agreement with reported values[37,38]. (**c**) Gas-hydrogenated $TiO_2$ with H staying at $V_O$ which corresponds to the minimum energy state. (**d**) Atom-hydrogenated $TiO_2$ with $H_i$. The insets of (**c**) and (**d**) show the PDOS of the hydrogen, respectively.

$TiO_2$ after a five-day aging. Therefore, the incorporated hydrogen in atom-hydrogenated $TiO_2$ is more diffusible and unstable than that in gas-hydrogenated $TiO_2$. By contrast, no such an absorption peak can be observed for the gas-hydrogenated samples.

Figure 2b presents optical absorption spectra of the samples. Upon hydrogenation or vacuum-annealing, the absorption edge shifts to the lower energy side and the absorption ratio for photons with lower energy than the absorption edge increases significantly. Meanwhile, colors of vacuum-annealed samples and the atom-hydrogenated $TiO_2$, turn from light yellow of blank sample to light blue (Fig. 2c) and the color of gas-hydrogenated sample becomes even dark blue, similar with the case of gas-hydrogenated anatase $TiO_2$ nanocrystals[10]. The valence-band (VB) spectra were measured by synchrotron radiation x-ray photoelectron spectroscopy (XPS) (Fig. 2d). For the vacuum-annealed and hydrogenated samples, the VB maximum lies at 2.6 eV and 1.4 eV, respectively, which are closer to the Femi level than blank sample as reported by Chen[10]. The results suggest a narrowing of the band gap, in agreement with the optical absorption measurements in Fig. 2b. Naldoni[16] and Zuo[31] regarded that $V_O$ contributed energy levels 0.7 ~ 1.0 eV below conduction band. Chen[10] and Naldoni[16] regarded that surface disorder contributed levels 2.0 eV below conduction band. In our VB spectra, we also observed a band 1.4 eV below Fermi level in samples annealed in 0.95 bar $H_2$ atmospheres. Instead, the VB position of the atom-hydrogenated $TiO_2$ was 2.5 eV. And the VB position of vacuum-annealed samples was also about 2.6 eV. These results made us propose that different hydrogen defects formed in different treatment methods. Furthermore, O-H bonds only formed in atom-hydrogenated $TiO_2$ but not in gas-hydrogenated samples. Instead, a large amount of $V_O$ and H defects coexisted in the gas-hydrogenated samples. Therefore we propose oxygen vacancies and hydrogen ions coexist independently or correlatedly in the gas-hydrogenated samples while only interstitial hydrogen atoms exist in the samples treated by electrochemical method. In order to understand different existing forms of hydrogen defects, we have turned to DFT calculations.

DFT calculations were carried out using the Vienna ab initio Simulation Program (VASP) code with projector-augmented-wave (PAW) pseudopotentials and the Perdew-Burke-Ernzerhof (PBE) exchange-correlation functional. The rutile $TiO_2$ structure was described as a $3 \times 3 \times 3$ supercell. First, the density of states (DOS) and the partial density of states (PDOS) of a perfect $TiO_2$ supercell (Fig. 3a) and the supercell with $V_O$ were calculated (Fig. 3b). As compared to the perfect $TiO_2$, the introduction of $V_O$ in the supercell results in two loosely captured electrons by three Ti dangling bonds. These two electrons can be transferred to Ti 3d states[32]. Then a H atom was incorporated in the supercell with $V_O$ and perfect supercell, respectively. It was found after structure optimization that the H atom added in the supercell with $V_O$ tends to reside on the $V_O$'s site as $H_O$ and the resulting lattice distortion becomes smaller than that with $V_O$ alone. This finding agrees with our synchrotron radiation x-ray diffraction results (Supplemental Fig. S3). The Fermi level for $TiO_2$ with $H_O$ also lies in the conduction band (CB) owing to the contribution of Ti 3d electrons (Fig. 3c). The inset shows that the states of $H_O$ contribute mainly to the VB. By contrast, H in the perfect $TiO_2$ prefers the interstitial site of oxygen octahedral as $H_i$, which is consistent with an earlier report[33]. The distance from $H_i$ to the closest O is found to be
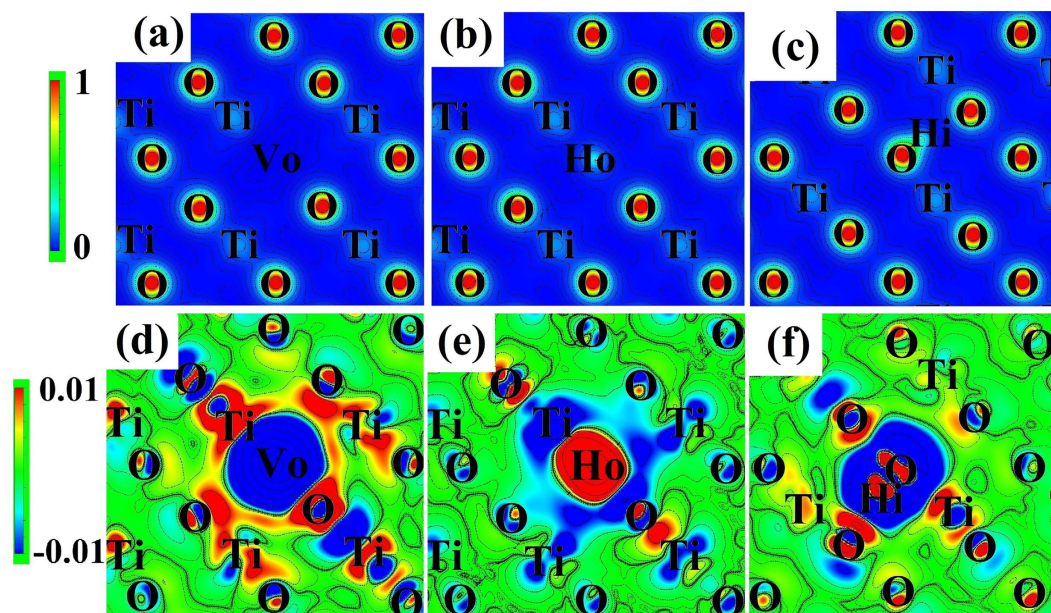
**Figure 4. Charge density and differential charge density for different configurations. (a–c)** is the charge density of the perfect $TiO_2$, $TiO_2$ with $V_O$, $TiO_2$ with $H_O$, and $TiO_2$ with $H_i$, respectively. **(d–f)** is the differential charge density of $TiO_2$ with $V_O$, $TiO_2$ with $H_O$, and $TiO_2$ with $H_i$, respectively. The blue color indicates the low electron density and the red color indicates the high electron density.

0.991 Å, very similar to the bond length of hydroxyl in $H_2O$. $H_i$ can also affect the Ti 3d band structure and move the Fermi level into the CB. The inset of Fig. 3d shows that some states of $H_i$ appear in the CB. Note that DOS of interstitial H is very small and only as 1% as that of H defects around Oxygen vacancies. In all these configurations, the VB and the CB are still primarily formed by O 2p and empty Ti 3d states, respectively. Hydrogen defects have little direct influence on the structure of VB or CB, contributing few DOS near the bandgap. However, they could modulate the structure of $TiO_2$ indirectly by their hybridization with O 2p and Ti 3d orbits. Chen[10] and Naldoni[16] proposed this shift was due to surface disorders. Here we tend to ascribe this shift in bulk and single crystalline $TiO_2$ to hybridization of H with O 2p orbits. This result agrees with our previous work[34].

The charge density and differential charge density analyses show that electrons move from $V_O$ to the neighboring Ti and O atoms in $TiO_2$ with $V_O$ (Fig. 4a,d). When H stays on the site of $V_O$, the neighboring Ti and O atoms give electrons to $H_O$, making $H_O$ negatively charged (Fig. 4b,e). Bader analyses also show that $H_O$ has 1.50 valence electrons (supplemental Table 1). In $TiO_2$ with $H_i$, the charge density of $H_i$ and the closest O atoms overlaps (Fig. 4c) and the charge density in between them is high (Fig. 4f), revealing the formation of a covalent bond, or specifically an O-H bond. The valence electron of $H_i$ is 0.35 and similar with that of H atoms in $H_2O$. These DFT calculations coincide well with our experimental observations of the appearance of the $3280\,cm^{-1}$ IR absorption peak in atom-hydrogenated $TiO_2$, but not in gas-hydrogenated $TiO_2$. Higher hydrogen contents in the supercell do not bring about significant charge density differences. Indeed, no experimental and theoretical evidences were found for the existence of O-H bonds in gas-hydrogenated $TiO_2$.

Annealing in vacuum and gaseous $H_2$ can both introduce a shallow donor state in rutile $TiO_2$ with nearly the same ionization energy of $6.5 \pm 1.5\,meV$. The $H_i$ alone in atom-hydrogenated $TiO_2$ also introduces a shallow donor, however, with lower ionization energy of $3.9\,meV$. Note that the $H_i$ is weakly bonded to the closest O atom and the resulted O-H bonds could be easily broken by high temperature annealing in air in short time or by several days' aging at RT[14]. This hydrogenation-derived O-H bonds behave quite differently from those inherent O-H defects in earlier studies in flame fusion-derived rutile $TiO_2$ crystals[28,29] or natural ores[35] which contained unavoidably large contents of OH defects, or the deuteration was carried out in $D_2O$ through isotope exchange[36]. Those inherent hydrogen defects were rather stable against high temperature annealing[26]. The $H_O$ defects, or the combination of H atoms with $V_O$ could stabilize the hydrogen atoms in $TiO_2$, making it insensitive to RT aging. Our study offers useful insights for studies of the interplay of hydrogen atmospheres and solid state oxide materials. We expect this research could contribute to the property tailoring of $TiO_2$ through appropriate hydrogen-related defect engineering.

## Methods

Rutile $TiO_2$ single crystals of (001)-orientation synthesized by floating zone method were used. All the samples were annealed in air at 700 °C for 120 hours to eliminate the native defects and reached a RT equilibrium resistivity of $(2.0 \pm 0.1) \times 10^8 \Omega$ cm. For high-temperature annealing, the samples were sealed in pre-evacuated quartz ampoules (background pressure $<1.0 \times 10^{-9}$ bar) with 99.999% $H_2$ of a RT pressure of 0, 0.05, 0.35 and 0.95 bar, respectively. Then the samples were annealed at 600 °C for 50 hours to reach their equilibrium state, followed by air quenching to RT. It is worth mentioning that the infrared spectra would be significantly affected by the hydroxyl pollution from quartz ampoules. The FTIR spectra obtained in the samples annealed in vacuum in normal quartz tubes also showed an observable absorption peak at 3280 cm$^{-1}$ (as shown in Supplemental Fig. S3). In order to avoid possible hydroxyl pollution from quartz ampoules, we have chosen dehydroxylated quartz ampoules. Furthermore, flame fusion-derived rutile $TiO_2$ single crystals unavoidably contained large contents of OH defects[28,29], so we chose the rutile single crystals synthesized by floating zone method. Moreover, high pressure hydrogen gas can also help to avoid hydroxyl pollution from quartz ampoules.

For comparison, interstitial hydrogen was introduced by atom-hydrogenation through electrolysis of 0.1 M $Na_2SO_4$ water solution at RT[22]. The $TiO_2$ chips were electroded by firing Ag pastes on parts of the chips. Atomic H was generated on the Ag electrode and then diffused into $TiO_2$ during the hydrogenation. The $TiO_2$ crystals became gradually blue and hydrogen started to form directly on the $TiO_2$ crystals. A surface layer of 50 μm thick was removed in order to keep the surface clean for following analyses.

The resistivity and Hall Effect of the samples were measured from 2 to 300 K by Physical Property Measurement System 9 (PPMS-9) and the current–voltage ($I$–$V$) characteristics were measured by Keithley 2400 using a four-electrode method. The oxygen loss was calculated through weight measurement using a micro-balance. The crystal structures were examined by synchrotron radiation x-ray diffraction (XRD) at 1W1A of Beijing Synchrotron Radiation Facility (BSRF). The optical absorption spectra of rutile $TiO_2$ samples were measured by Fourier-transform infrared spectrometer (Nicolet 6700) under transmission mode and Double beam UV-visible spectrophotometer (TU-1901) under reflection mode. The valence band structures were examined by synchrotron radiation XPS at 4B9B of BSRF. Hydrogen contents of samples were determined by diffusible hydrogen analyzer (Bruker-G4 Phoenix) at 700 °C.

The electronic structures of $TiO_2$ with different defects were calculated based on density functional theory (DFT) with the Perdew–Burke–Ernzerhof (PBE) exchange-correlation functional using the Vienna *ab initio* Simulation Program (VASP) code with projector-augmented-wave (PAW) pseudopotentials. The rutile $TiO_2$ structure was described as a $3 \times 3 \times 3$ supercell with 162 atoms consisting of a twelve-trilayer slab. The cutoff energy for expanding the Kohn-Sham wave functions was 400 eV. We used the experimentally derived lattice constants (a = b = 4.595 Å, c = 2.959 Å). All the atoms were fully relaxed without constraints until the forces were converged to 0.01 eV/Å. The Monkhorst-Pack $k$-point grid was $5 \times 5 \times 9$ for Brillouin zone integration of the supercell which was tested to be well converged.

## References

1. Walle, C. G. & Neugebauer, J. Universal alignment of hydrogen levels in semiconductors, insulators and solutions. *Nature* **423,** 626–628 (2003).
2. Janotti, A. *et al.* Hybrid functional studies of the oxygen vacancy in $TiO_2$. *Phys. Rev. B* **81,** 085212 (2010).
3. Kobayashi, Y. *et al.* An oxyhydride of $BaTiO_3$ exhibiting hydride exchange and electronic conductivity. *Nature Mater.* **11,** 507–511 (2012).
4. Tang, J., Durrant, J. R. & Klug, D. R. Mechanism of Photocatalytic Water Splitting in $TiO_2$. Reaction of Water with Photoholes, Importance of Charge Carrier Dynamics, and Evidence for Four-Hole Chemistry. *J. Am. Chem. Soc.* **130,** 13885–13891 (2008).
5. Fujishima A. & Honda K. Electrochemical photolysis of water at a semiconductor electrode. *Nature* **238,** 37–38 (1972).
6. Etgar, L. *et al.* Mesoscopic $CH_3NH_3PbI_3/TiO_2$ Heterojunction Solar Cells. *J. Am. Chem. Soc.* **134,** 17396–17399 (2011).
7. Kaden, W. E., Wu, T., Kunkel, W. A. & Anderson, S. L. Electronic structure controls reactivity of size-selected Pd clusters adsorbed on $TiO_2$ surfaces. *Science* **326,** 826–829 (2009).
8. Bavykin, D. V., Friedrich, J. M. & Walsh, F. C. Protonated titanates and $TiO_2$ nanostructured materials: synthesis, properties, and applications. *Adv. Mater.* **18,** 2807–2824 (2006).
9. Lee, J., Sorescu, D. C. & Deng, X. Electron-Induced Dissociation of $CO_2$ on $TiO_2$(110). *J. Am. Chem. Soc.* **133,** 10066–10069 (2011).
10. Chen, X. B., Liu, L., Yu, P. Y. & Mao, S. S. Increasing solar absorption for photocatalysis with black hydrogenated titanium dioxide nanocrystals. *Science* **331,** 746–750 (2011).
11. Wang, G. *et al.* Hydrogen-Treated $TiO_2$ Nanowire Arrays for Photoelectrochemical Water Splitting. *Nano Lett.* **11,** 3026–3033 (2011).
12. Lu, X. *et al.* Hydrogenated $TiO_2$ Nanotube Arrays for Supercapacitors. *Nano Lett.* **12,** 1690–1696 (2012).
13. Chester, P. F. & Bradhurst, D. H. Electrolytically Induced Conductivity in Rutile. *Nature* **199,** 1056–1057 (1963).
14. Chen, W. P., He, K. F., Wang, Y., Chan, H. L. W. & Yan, Z. J. Highly mobile and reactive state of hydrogen in metal oxide semiconductors at room temperature. *Sci. Rep.* **3,** 3149 (2013).
15. Liu, L., Yu, P. Y., Chen, X. B., Mao, S. S. & Shen, D. Z. Hydrogenation and Disorder in Engineered Black $TiO_2$. *Phys. Rev. Lett.* **111,** 065505 (2013).
16. Naldoni, A. *et al.* Effect of Nature and Location of Defects on Bandgap Narrowing in Black $TiO_2$ Nanoparticles. *J. Am. Chem. Soc.* **134,** 7600–7603 (2012).
17. DeFord, J. W. & Johnson, O. W. Electron transport properties in rutile from 6 to 40 K. *J. Appl. Phys.* **54,** 889–897 (1983).
18. Herklotz, F., Lavrov, E. V. & Weber, J. Infrared absorption of the hydrogen donor in rutile $TiO_2$. *Phys. Rev. B* **83,** 235202 (2011).
19. Kilic, C. & Zunger, A. n-type doping of oxides by hydrogen. *Appl. Phys. Lett.* **81,** 73–75 (2002).
20. Diebold, U. The surface science of $TiO_2$. *Surf. Sci. Rep.* **48,** 53–229 (2003).
21. Diebold, U., Li, S. C. & Schmid, M. Oxide surface science. *Annu. Rev. Phys. Chem.* **61,** 129–148 (2010).

22. Wang, Z. T., Deskins, N. A., Henderson, M. A. & Lyubinetsky, I. Inhibitive influence of oxygen vacancies for photoactivity on TiO$_2$ (110). *Phys. Rev. Lett.* **109,** 266103 (2012).
23. Yagi, E., Hasiguti, R. R. & Aono, M. Electronic conduction above 4 K of slightly reduced oxygen-deficient rutile TiO$_{2-x}$. *Phys. Rev. B* **54,** 7945–7956 (1996).
24. Zhai, T. *et al.* Oxygen vacancies enhancing capacitive properties of MnO$_2$ nanorods for wearable asymmetric supercapacitors. *Nano Energy* **8,** 255–263 (2014).
25. Filippone, F., Mattioli, G., Alippi, P. & Bonapasta, A. A. Properties of hydrogen and hydrogen-vacancy complexes in the rutile phase of titanium dioxide. *Phys. Rev. B* **80,** 245203 (2009)
26. Sze, S. M. & NG, K. K. *Physic of semiconductor devices* Ch. 1 (John Wiley & Sons, Inc. Press, New York, 2006).
27. Shu, D. J., Ge, S. T., Wang, M. & Ming N. B. Interplay between external strain and oxygen vacancies on a Rutile TiO$_2$ (110) surface. *Phys. Rev. Lett.* **101,** 116102 (2008).
28. Soffer, B. H. Studies of the optical and infrared absorption spectra of rutile single crystals. *J. Chem. Phys.* **35,** 940–945 (1961).
29. Johnson, O. W., Ohlsen, W. D. & Kingsbury, P. I. Defects in rutile. III. Optical and electrical properties of impurities and charge carriers. *Phys. Rev.* **175,** 1102–1109 (1968).
30. Chen, W. P. *et al.* Spontaneous recovery of hydrogen-degraded TiO$_2$ ceramic capacitors. *Appl. Phys. Lett.* **84,** 103–105 (2004).
31. Zuo, F. *et al.* Self-Doped Ti$^{3+}$ Enhanced Photocatalyst for Hydrogen Production under Visible Light. *J. Am. Chem. Soc.* **132,** 11856–11857 (2010).
32. Ganduglia-Pirovano, M. V., Hofmann, A. & Sauer, J. Oxygen vacancies in transition metal and rare earth oxides: Current state of understanding and remaining challenges. *Surf. Sci. Rep.* **62,** 219–270 (2007).
33. Koudriachova, M. V., Leeuw, S. W. & Harrison, N. M. First-principles study of H intercalation in rutile TiO$_2$. *Phys. Rev. B* **70,** 165421 (2004).
34. Mo, L. B. *et al.* Band gap engineering of TiO$_2$ through hydrogenation. *Appl. Phys. Lett.* **105,** 202114 (2014).
35. Maldener, J., Rauch, F., Gavranic, M. & Beran, A. OH absorption coefficients of rutile and cassiterite deduced from nuclear reaction analysis and FTIR spectroscopy. *Miner. Petrol.* **71,** 21–29 (2001).
36. Spahr, E. J. *et al.* Giant enhancement of hydrogen transport in rutile TiO$_2$ at low temperatures. *Phys. Rev. Lett.* **104,** 205901 (2010).
37. Pan, H., Zhang, Y. W., Shenoy, V. B. & Gao H. J. Effects of H-, N-, and (H, N)-doping on the photocatalytic activity of TiO$_2$. *J. Phys. Chem. C* **115,** 12224 (2011).
38. Shirly, R., Kraft, M. & Inderwildi, O. R. Electronic and optical properties of aluminium-doped anatase and rutile TiO$_2$ from ab initio calculations. *Phys. Rev. B* **81,** 075111 (2010).

## Acknowledgements

## Author Contributions

L.B.M. conducted the experiments and computations and contributed to writing of the manuscript. Y.W. and C.H.W. contributed to the design of the study and writing of the manuscript. Y.B., Q.Y.X. and Q.L. contributed to the experiments. W.Q.Y. did XPS and AES analyses. J.O.W. and I.K. conducted XPS analyses at BSRF. H.H.W. did XRD measurements at BSRF. J.L.C. designed the study and wrote the manuscript.

## Additional Information

**Supplementary information** accompanies this paper at http://www.nature.com/srep

**Competing financial interests:** The authors declare no competing financial interests.

**How to cite this article**: Mo, L.-B. *et al.* Hydrogen Impurity Defects in Rutile TiO$_2$. *Sci. Rep.* **5,** 17634; doi: 10.1038/srep17634 (2015).